Computation of the conditions for anti-angiogenesis and gene therapy synergistic effects: Sensitivity analysis and robustness of target solutions

Abdoulaye Diouf, Houda Mokrani, Evans Afenya, Baba Issa Camara

Version of Record: https://www.sciencedirect.com/science/article/pii/S0022519321002691
Manuscript_90665e1d5ec4376855c20bc4a94d5e53

Computation of the conditions for anti-angiogenesis and gene therapy synergistic effects: sensitivity analysis and robustness of target solutions

A. Diouf[b], H. Mokrani[b], E. Afenya[c], B. I. Camara[d,*]

[a] *Université Assane Seck de Ziguinchor,*
Laboratoire de Mathématiques & Applications
Route de Diabir, BP: 523 Ziguinchor, SENEGAL
[b] *Université de Rouen - CNRS UMR 6085*
Laboratoire de Mathématiques Raphaël Salem
Avenue de l'Université, 76801 Saint-Étienne-du-Rouvray, France
[c] *Department of Mathematics, Elmhurst University,*
190 Prospect Ave., Elmhurst, IL 60126, USA
[d] *Université de Lorraine - CNRS UMR 7360*
Laboratoire Interdisciplinaire des Environnements Continentaux
Campus Bridoux - 8 Rue du Général Delestraint, 57070 Metz, France

Abstract

Both anti-angiogenesis and gene therapy involve complex processes depending on non-point parameters belonging to a space of values. To successfully overcome the challenges involved in their therapeutic approaches, there is a need to analyze the sensitivity of these parameters. In this paper, a new mathematical model that combines immune system stimulations, inflammatory processes associated with tumor development, and gene therapy aimed at enhancing the efficacy of both treatments are explored. Using the global sensitivity methods of Sobol and Morris, the most important parameters are estimated. Estimation of the sensitivity variance revealed a strong interdependence between the parameters. Also, determinations of the conditions for effective therapy lead to a target of reducing the cancer cell numbers by at least 50%. This opened the way for delimiting the parameter spaces making it possible to reach the treatment target in addition to enhancing

*Corresponding author
Email addresses: abdoulayediouf333@gmail.com (A. Diouf), houdamokrani@yahoo.fr (H. Mokrani), evansa@elmhurst.edu (E. Afenya), baba-issa.camara@univ-lorraine.fr (B. I. Camara)

the estimation of the minimum time of remission. The combination of therapies and sensitivity analysis have demonstrated the robustness of therapy success.

Keywords: Cancer gene therapy, Oncolytic viruses, Inflammation, Mathematical model, isobologram analysis

1. Introduction

Cancer gene therapy is a promising treatment strategy. Advances in knowledge of the biology of viruses have been used to consider replicating vectors preferentially in tumors that can significantly amplify the expression of gene therapy. Among these viruses, some have a mutation or a deletion in their genome that affect replication in normal cells but not in cancer cells. However, although much progress has been made in both the theoretical study and clinical trials of oncolytic viruses [13, 17, 43, 51, 52, 54, 55], problems still remain to be addressed with regards to their interactions with the host immune response to virus-infected tumor cells [29, 50] or the tumor microenvironment [4].
Inflammation in the tumor-microenvironment has gained prominent attention as a potential critical player in tumor metastasis. An inflammatory tumor microenvironment fosters tumor growth, angiogenesis, and metastasis progression. Inflammation is an advantage for the tumor since an important part of the inflammatory process is dedicated to the reconstruction of the tissue, which also requires mechanisms involved in tumorigeneses. Tumor inflammation is induced by inflammatory factors secreted by tumor cells, such as the platelet-derived growth factor-D (PDGF-D) that recruits macrophages within the tumor, thus behaving as a powerful tumor promoter: it allows a faster progression of oncogenesis [46]. Proliferation and survival, which are already over-activated in cancer cells, are stimulated by inflammation.
Angiogenesis, which is absolutely necessary for tumor growth, is induced by inflammation [3, 45]. Targeting angiogenesis can be an effective approach to prevent the development of new blood vessels and is an essential modality for normalizing the tumor-associated vasculature [1]. As a result, the irregular vasculature leads to impaired tumoral blood flow that cannot supply nutrient to cells, remove waste products, and this causes significant fluctuations within the tumor microenvironment [5, 10, 20, 23]. Oncolytic viruses have been recognized as offering the possibility of targeted delivery of angiogenesis inhibitors, and recent studies have uncovered anti-angiogenic effects of oncolytic viral ther-

apy on tumoral angiogenesis that is in effect backed by inflammatory processes, [2, 7, 8, 11, 21, 37, 47, 57].
To explore the role of inflammation in cancer, Wilkie and Aktar [49] proposed a model for inflammation-driven stimulation of tumor growth through increases to the environmental carrying capacity. Their model takes into account the formulation derived by Hahnfeldt et al.[22], which provide a time-dependent carrying capacity for cancer under angiogenic control.
In this article, we model the interaction between the susceptible and infected tumor cells, the onclyotic virus and a time dependence of the cancer carrying capacity. Therefore, our model also incorporates the time-dependent resources available to the tumor system, the antitumoral and antiviral immune responses, following an initial successful viral propagation phase on tumor cell populations. The other variables appearing in our model come from a modification of models introduced by Mahasa et al. [27] and Storey et al. [41].
It is known that model outputs often have complex, nonlinear relationships with model parameters [30, 34, 53]. To avoid bias in model outputs from inappropriate choices of parameter values, we evaluate the performance of two well-known methodologies for sensitivity analysis. The model sensitivities can be defined as the derivatives of the solution with respect to the parameters. It contains two major goals: on the one hand, the sensitivities serve as diagnostics for the model, very useful for understanding how changes in the parameters induce effects on the model. On the other hand, this approach is due to the usefulness of derivatives in many circumstances. In the scientific literature, three types of sensitivity analyzes are frequent: local sensitivity analysis, assistant sensitivity analysis and methods of global sensitivity analysis. The local sensitivity analysis is known for its character of directly giving the gradient of the solution with respect to each parameter along the time series. It can be costly for larger models. Comparatively, the methods of global sensitivity analysis (GSA) are most appropriate for determining the important parameters that dominate model predictions. GSA can also estimate the magnitude of hidden bias that would need to be present to alter the conclusions of an observational study. In this paper, we mainly focus on two common methods of global sensitivity analysis: the Morris and Sobol methods [31, 40]. For more details on the implementations of these two global analysis methods, see [38, 53].
Finally, we use a similar approach developed in [12, 44], as in the isobole determination of effective concentration (EC_x) in a mixture

dose-response relationship, (EC_{50} ($x = 50$) are concentrations inducing 50% response). That is to say, we determine the model parameter spaces leading to a synergy of the two therapeutic approaches with 50% reduction in the population of cancer cells. Synergy indicates that two or more components are mixed together, and the effect is greater than the sum of the effects of the individual components when applied alone.

2. Material and Methods

2.1. The Mathematical Model

The model describes the interactions between tumor cells (i.e. infected plus uninfected) in the presence of the adaptive immune responses following an initial successful viral propagation phase on tumor cell populations within intratumoral delivery [42] and by assuming that viral particles and cells follow mass action kinetics, and all cell populations are homogenously mixed [6]. In this model, the growth of tumor cells (i.e. infected plus uninfected) within an inflammatory environment is stimulated by the immune system through an inflammatory process incorporated in the carrying capacity K_T. The model takes into account the dynamical interactions between a population of susceptible and uninfected tumor cells, $T_S(t)$; a population of infected tumor cells, $T_I(t)$; a population of oncolytic viruses $V(t)$; the tumor-specific immune cells $Y_T(t)$; the virus-specific immune cells $Y_V(t)$ and the carrying capacity $K_T(t)$. When the oncolytic virus is administered, the dynamical interactions between the virus and tumor cell population is described by the following system of equations in the tumor region Ω,

$$\frac{dT_S}{dt} = r_T T_S\Big(1 - \frac{T_S + T_I}{K_T(t)}\Big) - \beta_T T_S V - \gamma_T \frac{Y_T}{h_Y + Y_T} T_S, \tag{1a}$$

$$\frac{dK_T}{dt} = p(T_S + T_I) - qK_T(T_S + T_I)^{2/3}, \tag{1b}$$

$$\frac{dT_I}{dt} = \beta_T T_S V - \lambda_T T_I - \gamma_T \frac{Y_T}{h_Y + Y_T} T_I - \gamma_V Y_V T_I, \tag{1c}$$

$$\frac{dV}{dt} = b_T \lambda_T T_I - \omega V, \tag{1d}$$

$$\frac{dY_T}{dt} = p_T \frac{T_S + T_I}{h_T + T_S + T_I} - \delta_T Y_T, \tag{1e}$$

$$\frac{dY_V}{dt} = p_V T_I(t - \tau) - \delta_V Y_V. \tag{1f}$$

Each equation describes the rate of change in hours of the population of a single cell type or of the virus. Time $t = 0$ represents the time at which the initial viral dose is administered. We assume that there are no new immune cells being recruited to target the tumor at the time of the initial viral dose. We start simulations with the initial conditions $T_S = 10^6$ cells and $V = 10^7$ pfu (plaque-forming units). Virions that are incapable of forming plaques cannot infect their target cells, and are excluded when counting the plaque-forming units [28]. All other cell populations begin at 0 and for $\tau \leq t \leq 0$, we have constant history functions of cell concentrations on that time interval.

2.2. Biological Motivations Behind the Model

The model is explained as follows. *During oncolytic virotherapy, the tumor cell population is sub-divided into two sub-populations, the uninfected tumor cells represented by T_S and infected tumor cells denoted by T_I.* The susceptible (uninfected) tumor cells grow logistically at the rates, r_T, up to their carrying capacities, K_T.

When the oncolytic virus meets susceptible tumor cells, infection can occur at a rate β_T. The interaction between tumor and the tumor-specific immune cells follows the Michaelis-Menten kinetics, $\gamma_T \frac{Y_T}{h_Y + Y_T} T_S$, because immune cell infiltration into the tumor is often restricted by tumor architecture [24]. Thus, γ_T denotes the rate at which tumor cells are lysed by the tumor-specific immune cells and h_Y represents the half-saturation constant of immune cells that supports half the maximum killing rate.

The equation (1b) is derived from the model of Hahnfeldt et al. [22], where the effective vascular support of the tumor microenvironment, or carrying capacity, grows in a time-dependent manner with the tumor mass. The first term $p(T_S + T_I)$ represents the stimulatory capacity of the tumor upon the inducible vasculature (through, e.g., angiogenic factors like vascular endothelial growth factor) and the second term $qK_T(T_S + T_I)^{2/3}$ reflects endogenous inhibition of previously generated vasculature (through, e.g., endothelial cell death or disaggregation). The main conclusion of their work was that the ratio of the second term should be proportional to the tumor volume raised to the power 2/3.In the equation (1b), p is the stimulation coefficient and q is the inhibition coefficient.

For infected cell populations T_I, we assume that their lifespan is much shorter than uninfected cell populations; hence, we do not need logistic growth. The equation (1c) models the infected tumor population, in which term $\beta_T T_S V$ denotes the addition of cells to the population T_I

via viral infection of susceptible tumor cells at rate β_T, and $-\lambda_T T_I$, denotes the death of the infected tumor cells.
Again, since tumor architecture may hinder the adaptive antitumor immune cell infiltration [24], the interaction between the infected tumor cells and the adaptive antitumor immune response is modeled with the term $\gamma_T \frac{Y_T}{h_Y + Y_T} T_I$. The last term, $-\gamma_V Y_V T_I$, represents the number of infected tumor cells that become lysed by the virus-specific immune cells.

Equation (1d) models the oncolytic virus population, with the first term $b_T \lambda_T T_I$ representing the addition of new viral particles that are released when an infected tumor cell lyses. The parameter b_T denotes the viral burst size released from each infected cell. The final term ωV, corresponds to clearance of the viral particles, resulting from local non-specific immune cells in the tumor region.

Equation (1e) models the tumor-specific adaptive immune response. We assume that tumor-specific immune cells can recognize and kill both uninfected and infected tumor cells because tumors often express tumor-associated antigens [9]. The first term, $p_T \frac{T_S + T_I}{h_T + T_S + T_I}$, represents the antitumoral immune response, propelled by pro-tumoral inflammatory behaviors [21] against the tumor cells, with the immune cell recruitment rate p_T, and the half-saturation constant h_T. Finally, the last term, $-\delta_T Y_T$, denotes that the adaptive tumor-specific immune population declines as a result of natural cell death, at the intrinsic death rate δ_T.

Equation (1f) models the adaptive virus-specific immune response. We assume that the immune response to viral antigens require time necessary for cell activation and proliferation. That means, antigenic stimulation generating the antiviral immune response, mediated by T cells, require a period of time τ, which may depend on prior antigenic stimulation period $t - \tau$. So, the first term $p_V T_I(t - \tau)$, represents the delayed immune response to virus infection to tumor cells, where a parameter p_V is a virus-specific proliferative rate of the antiviral immune cells due to the presence of virus particles (virus antigens) on the surface of the infected cells. The last term, $-\delta_V Y_V$, represents the natural death, with the death rate δ_V.
The summary of the parameter ranges is presented in Table 1.

Table 1: Parameter values used in the model simulations.

Parameter	Description	Value	Range	Source
r_T	the intrinsic growth rate of tumor cells	0.003 hr^{-1}	$(0.01 - 0.3)$ hr^{-1}	[35, 55]
β_T	the rate at which virus infects tumor cells	4×10^{-11} $virion^{-1}$ hr^{-1}	$(4 \times 10^{-12} - 8 \times 10^{-6})$ $virion^{-1}$ hr^{-1}	[35]
γ_T	lysis rate of susceptible tumor cells by tumor-specific immune cells	1/24 hr^{-1}	$(10^{-9} - 0.50)$ hr^{-1}	[16]
h_Y	the half-saturation constant of immune cells	40.0 cells	$(0.01 - 50.01)$ cells	[16]
γ_V	lysis rate of the infected normal cells by virus-specific immune cells	1/24 $cells^{-1}$ hr^{-1}	$(5 \times 10^{-13} - 0.1)$ $cells^{-1}$ hr^{-1}	[27]
λ_T	death rate of infected tumor cells due to virus lysis	1/24 $cells^{-1}$ hr^{-1}	$(10^{-8} - 0.5)$ $cells^{-1}$ hr^{-1}	[16]
b_T	the burst size from tumor cells lysed by virus	1350 virions $cell^{-1}$	$(400.0 - 7400)$ virions $cell^{-1}$	[35]
ω	virus clearance rate	0.025 hr^{-1}	$(0.001 - 0.25)$ hr^{-1}	[18, 36]
δ_T	death rate of the tumor-specific immune cells	0.000375 hr^{-1}	$(0.00000375 - 0.0375)$ hr^{-1}	[15]
h_T	the half-saturation constant of tumor cells in response to tumor antigens	40 cells	$(0.01 - 50.01)$ cells	[16]
p_V	proliferation rate of virus-specific immune cells in response to virus antigens	0.055 hr^{-1}	$(0.01 - 0.3042)$ hr^{-1}	[16]
p_T	proliferation rate of tumor-specific immune cells	0.0375/24 hr^{-1}	$(0.00015 - 0.015)$ hr^{-1}	[27]
τ	the delay time	8 hr	$(5 - 10)$ hr	[27]
δ_V	death rate of the virus-specific immune cells	0.00554 hr^{-1}	$(0.0001 - 0.0554)$ hr^{-1}	[16]
p	the stimulation coefficient	0.008 hr^{-1}	$(0.001 - 2.00)$ hr^{-1}	[48]
q	the inhibition coefficient	7.0×10^{-5} $(cell\ no.)^{-2/3}$ hr^{-1}	$(0.05 \times 10^{-5} - 40 \times 10^{-5})$ $(cell\ no.)^{-2/3}$ hr^{-1}	[48]
$K_{T,0}$	the carrying capacity of tumor cells	1.47×10^8 $(cell\ no.)$	$(1.72 \times 10^4 - 2.46 \times 10^8)$ $(cell\ no.)$	[48]

2.3. Computation methods of sensitivity analysis

The Sobol method [40] is a variance-based computation and breaks the variance of the model or system output into fractions that can be assigned to inputs or sets of inputs. This helps to not only obtain the sensitivities of the individual parameters, but also provides a means of quantifying the effect and sensitivity of the interaction between the parameters. Let the model be represented by a function

$$Y = f(X) = f(X_1, \ldots, X_d),$$

where Y is the model output and $X = (X_1, \ldots, X_d)$ is the parameter set. Sobol suggested to decompose the function f into summands of increasing dimensionality:

$$Y = f_0 + \sum_{i=1}^{d} f_i(X_i) + \sum_{i<j}^{d} f_{ij}(X_i, X_j) + \cdots + f_{1,2,\cdots,d}(X_1, X_2, \cdots, X_d)$$

The attribution of total output variance to individual model parameters and their interactions can be written as:

$$Var(Y) = \sum_{i=1}^{d} V_i + \sum_{i<j}^{d} V_{i,j} + \cdots + V_{1,2,\cdots,d},$$

where $Var(Y)$ represents the total variance of the output metric Y ; V_i is the first-order variance contribution of the i-th parameter, $V_{i,j}$ is the second-order contribution of the interaction between parameters i and

j; and $V_{1,2,\cdots,d}$ contains all interactions higher than third-order, up to d total parameters. In this study, each parameter's total sensitivity index is used (i.e., its individual effects plus an estimate of its interactions with all other parameters).

The Sobol indices are "ordered", the first order indices given by $S_i = \dfrac{V_i}{Var(Y)}$ is the fraction of the total output variance caused by the parameter i. It is a measure for the variance contribution of the individual parameter X_i to the total model variance. It is normalized by the total variance to provide a fractional contribution. Higher order interaction indices $S_{i,j}$, $S_{i,j,k}$ and so on can be formed by dividing other terms in the decomposition of the variance by $Var(Y)$.
Sensitivity indices are approximated using numerical integration in a Monte Carlo framework. A global sample of the parameter space is taken using a quasi-random Sobol'sequence of values to achieve a uniform coverage of the space. The parameter sets generated from these sampling ranges are evaluated in the model, creating a distribution of output values, Y , which have a total variance D as follows:

$$\begin{aligned} Y_0 &= \frac{1}{n}\sum_{s=1}^{n} Y(\theta_s) \\ D &= \frac{1}{n}\sum_{s=1}^{n} Y^2(\theta_s) - Y_0^2, \end{aligned}$$

where Y_0 is the mean of the distribution of model outputs and θ_s represents the parameter set associated with sample s.

Parameter ranges used Sobol methods are listed in Table 1.

2.4. Computation methods for the determination of effective parameter values

In each of our simulations to determine the space of parameter values for which we observe synergistic effects of anti-angiosenesis and gene therapy combination, we choose two varying control parameters from our model (one is linked to the anti-angiosenesis and the other to gene therapy). The rest of the other model parameters are fixed when the model control parameters vary. We assume that the initial amount of cancer cells exceeds 10^6. For a given couple of control parameter pair, we observe the model output in a period of 200 hours. If over the last 100 hours of observation, the quantity of cancer cells is below 50% of their initial size, then the value of the control parameter pair becomes

an effective control value. This effective control value is thus saved as well as the minimum time to observe for the first time a 50% decrease in cancer cells.

3. Results

In Figure 1 and Figure 2, we represent from the second line of the times column, the dynamics of the six populations studied. The figures on the diagonal represent the distribution of the observed values for a given variable. The rest of the other figures represent all the phase portrait couples of the five populations. The values on the upper diagonal represent the associated correlations. The model parameters were set as follows in (2):

$$\begin{aligned} r_T = 0.15 \quad &, \ \beta_T = 8e-11, \ \gamma_T = 0.3, \ h_Y = 15.0, \\ p = 0.06 \quad &, \ \gamma_V = 0.001, \ b_T = 1800, \ \omega = 0.15, \ \lambda_T = 0.0001 \\ p_T = 0.005 \quad &, \ h_T = 22, \ \delta_T = 0.0075, \ p_V = 0.15, \ \delta_V = 0.0155 \end{aligned} \tag{2}$$

In Figure 1, we fix the inhibition coefficient $q = 4e^{-5}$, leading to slow down of cancer cells. While in Figure 2, q is fixed as $q = 0.01e^{-5}$ which leads to the failure of virotherapy.

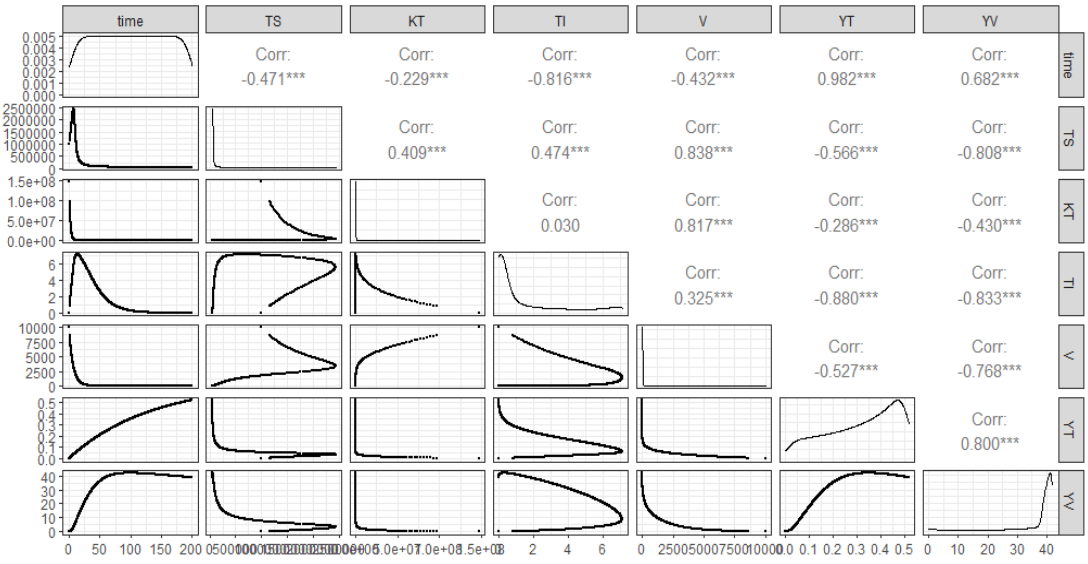

Figure 1: Population dynamics with cancer cell extinction, phase portraits and correlation when all the parameters are fixed as in (2) except $q = 4e^{-5}$.

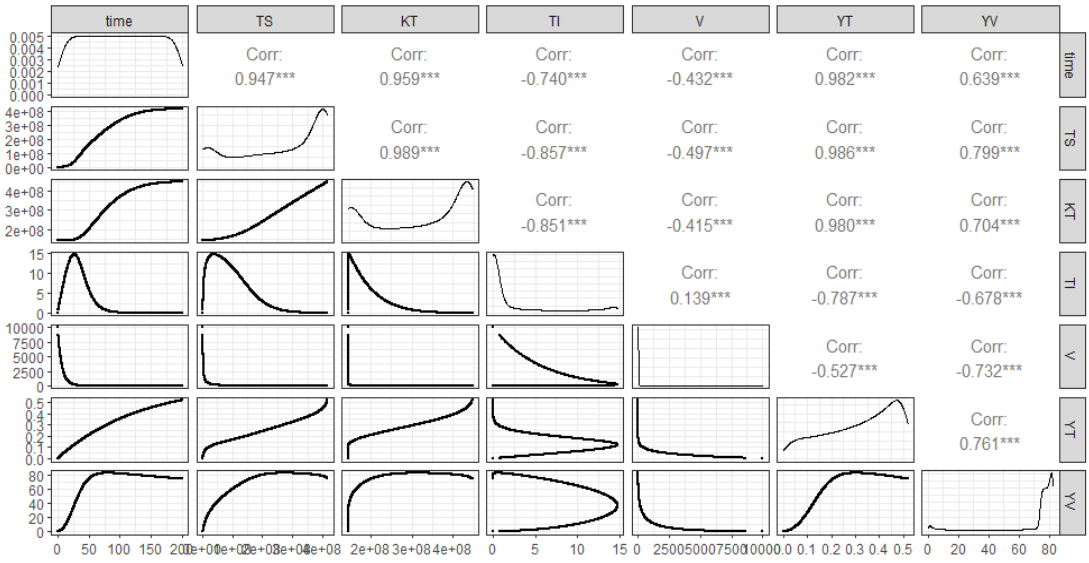

Figure 2: Population dynamics with cancer cell persistence, phase portraits and correlation when all the parameters are fixed as in (2) except $q = 0.01e^{-5}$.

3.1. Computation of the sensitivity of model parameters

Global sensitivity analysis (GSA) of the model was performed using the variance-based Sobol method [39, 40]. Model output variances were estimated using Monte Carlo integrals. So a critical step of sampling-based GSA is therefore the choice of the sample size to run the Monte Carlo experiment.

The total cost of this analysis is $N = (p + 2) \times n$ model evaluations (where p is the number of factors and n is the random sample size). The generation of this set of model runs of size N is by far the most computationally demanding step in the calculation of variance- based indices. The aim is therefore to pick the minimum n needed to ensure our index calculation is reliable. Based on the work of Nossent et al. [33], we found that the sample size n is 10800, resulting in 194,400 model evaluations to calculate the first order and total sensitivity index. Results of convergence analysis across the GSA method was performed with the Python software package "SALib".

In Figure 3, the sensitivity analysis showed that the inhibition coefficient q is strongly influenced by the population of susceptible and uninfected tumor cells $T_S(t)$, for all time points. It has 2 times more influence on the total variance than the second and third ranked pa-

rameters, r_T (the intrinsic growth rate of uninfected tumor cells) and p (the stimulation coefficient).

At the very beginning, the parameter r_T occupied this place but quickly decreases with an exponential speed after 75 hours of observation period, which suggest the importance of the effects of the inflammatory environment. Indeed, the parameter q is the factor involving the most non-linear interactions unlike the rest of the parameters, throughout the study duration.

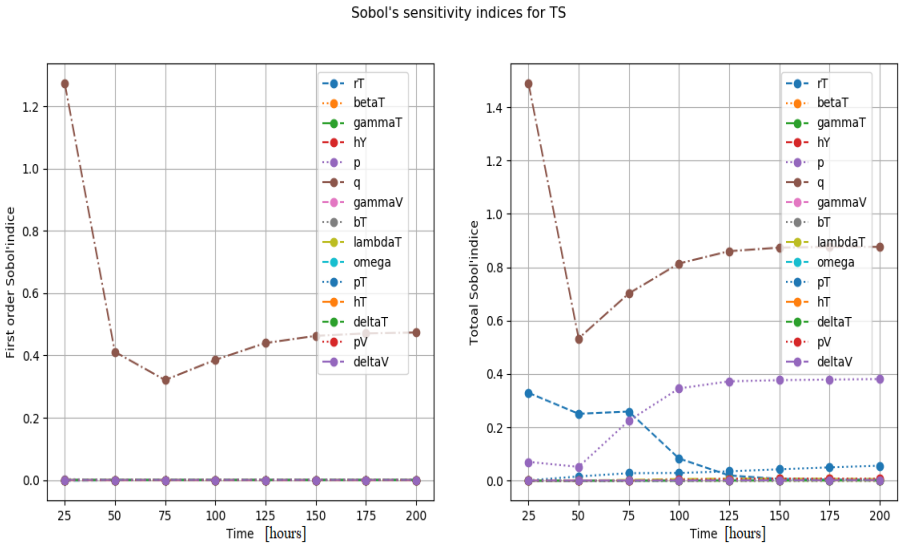

Figure 3: Sobol sensitivity indices for T_S state variable

As seen in Figure 4, the inhibition coefficient q is the single most influential parameter in addition to being an important factor of variability for non-linear interactions on the load capacity K_T. At the same time, q and p are parameters that induce the most residual variability due to interactions between the fixed parameter X_i and the other parameters (see the right of Figure 4).

With regard to the population of infected tumor cells $T_I(t)$, Figure 5 shows that q is the most influential parameter from the first 65 hours. However after $t = 65$ hours, q lost its global influence on $T_I(t)$ to the detriment of p_V, the proliferation rate of virus- specific immune cells in reponse to virus antigens. In addition, p_V, λ_T (the death rate of infected tumor cells due to virus lysis) and q represent the parameters which involve the most interactions and non- linearities on the dynamics of $T_I(t)$. We note that the estimates of the first-order Sobol's index of

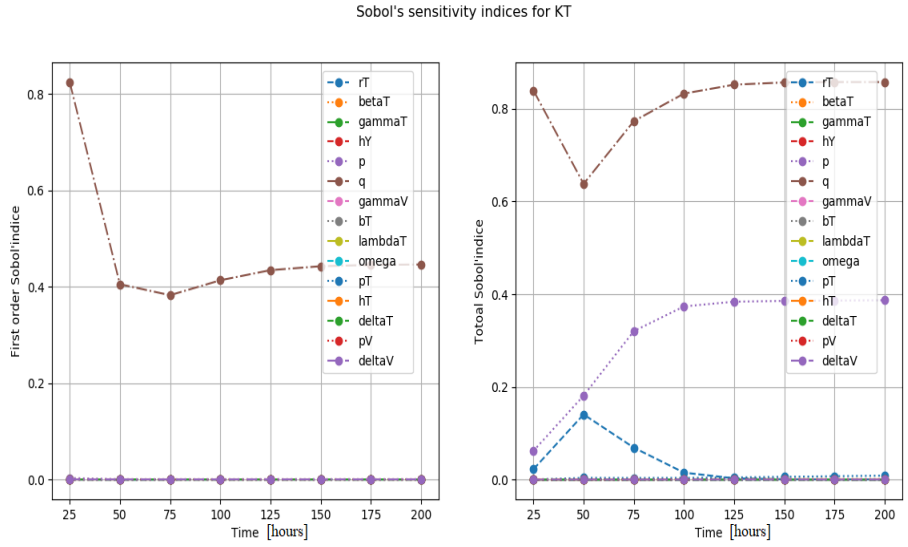

Figure 4: Sobol sensitivity indices for K_T state variable

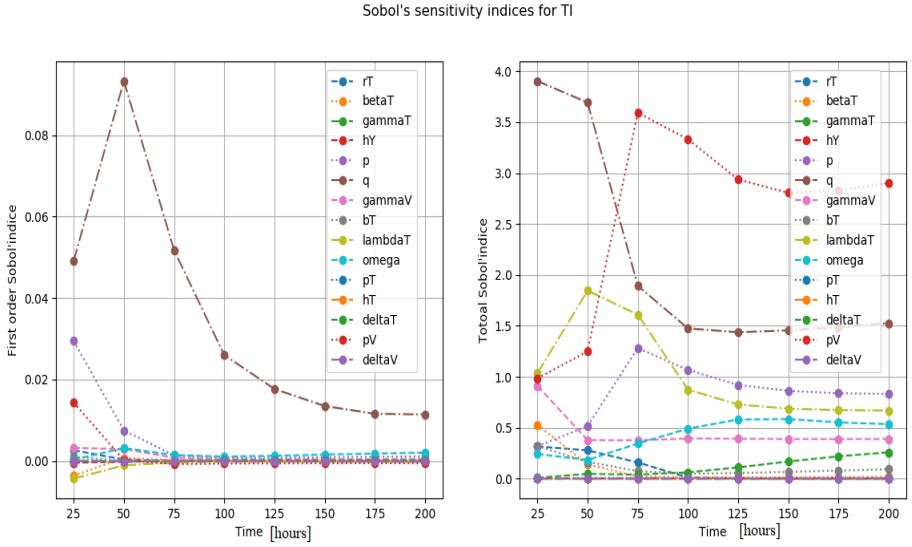

Figure 5: Sobol sensitivity indices for T_I state variable.

λ_T and β_T are slightly negative, which may occur when the indices do not significantly differ from 0. Also, it is important to note strong variability induced by almost all the parameters from 50 hours to 160 hours.

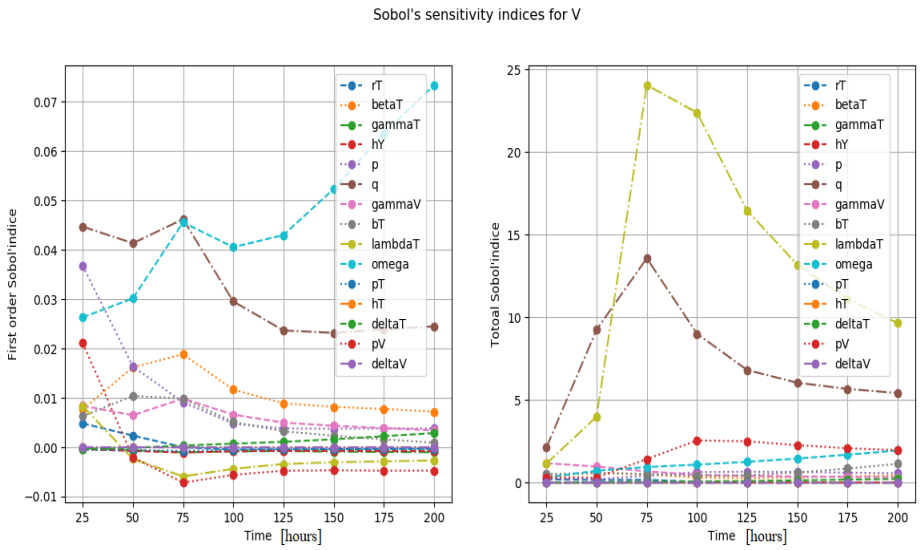

Figure 6: Sobol sensitivity indices for V state variable

With regard to the free virus population $V(t)$, Figure 6 shows that q is the most influential parameter from the first 60 hours. After $t = 60$ hours, q lost its global influence to the detriment of λ_T. However, total effect of λ_T is slightly higher than the main effect signifying that there is little interaction with other parameters. On other hand, the virulence rate ω and q are those which contributed the most on the non-linearity or the level of interaction of their influences on V.

In Figure 7, p_T and δ_V are far from the parameters that most affect the tumor-specific immune cells $Y_T(t)$, and since the difference between the total effect index and main effect index of each parameter appear similar it can be assumed they are interacting parameters. This corroborates the idea that increased efficacy depends on the combination of virus and immune response [19].

Figure 8 shows us that p and q have the greatest overall influence on the immune cells specific for the virus $Y_V(t)$, followed by w, λ_T and γ_V, in the order of listing.

3.2. Computation of effective control paramater space

This section presents the simulations to show where, both in time, space and in parameter space, 50% of cancer size reduction exists. In each graph of Figure 9, we have two regions: one in gray where the target

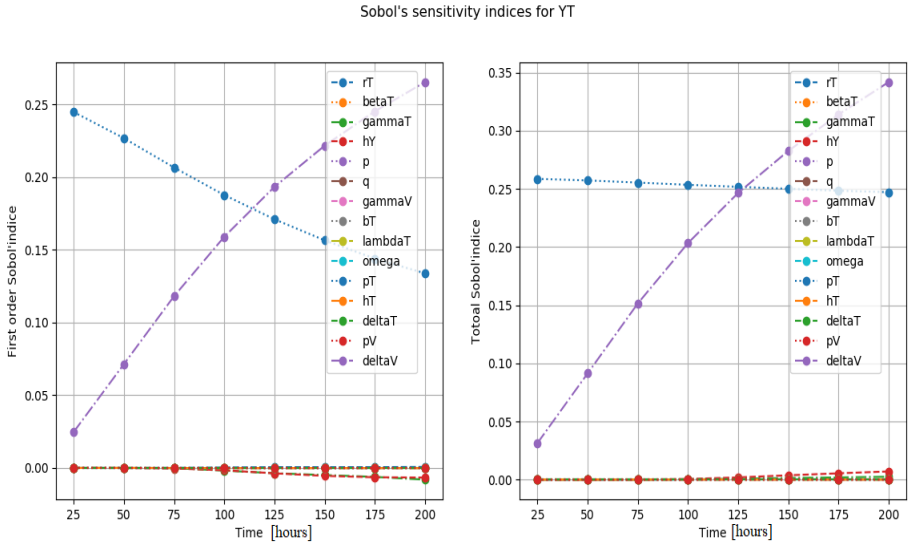

Figure 7: Sobol sensitivity indices for Y_T state variable

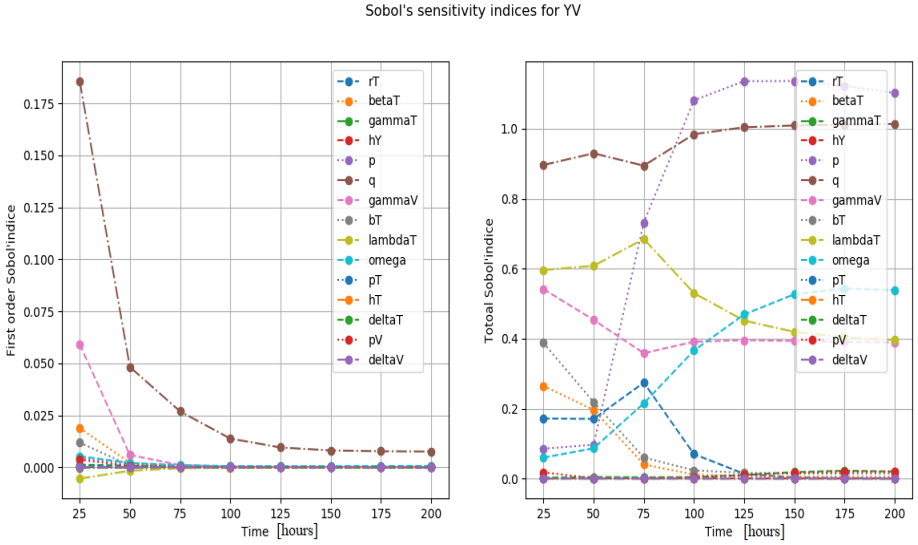

Figure 8: Sobol sensitivity indices for Y_V state variable

of cancer reduction is not reached and one with color palettes varying from blue to red where the target is reached. The color palette represents the minimum time for the quantity of tumor cells to be reduced by 50%: the red color corresponds to a longer minimum time and the

blue color is for a shorter minimum time. Therefore, the simulations of our model that combines anti-angiogenic treatment with gene therapy shows the existence of effective model parameters inducing 50% of cancer size reduction. Furthermore we observe, at the limits of the reduction target regions, a non-linear relation of the critical values of control parameter pairs. By considering, in Figure 9(A), the couple(b_T, h_Y)as a control parameter pair, we observe a parabolic covex curve that delimits the upper limit of the region where the cancer reduction target is reached. The minimum time (> 50 hours) to reach the target is longer (red or yellow color) for low values of b_T and h_Y. However, this minimum time becomes lower (< 25 hours, blue color) as soon as $b_T > 5700$. In Figure 9(B), (β_T, p) is chosen as representative control parameter pair. The obtained shape of the 50% reduction region is similar to that of the pair (b_T, h_Y). The minimum control time is more than 10 hours if $\beta_T < 5 \times 10^{-10}$ while it becomes less than 5 hours as soon as $\beta_T > 6 \times 10^{-10}$. In Figure 9(C), ($\gamma_T$, q) is the ccontrol parameter pair. The reduction target of the cancer cells is not reached in the gray region where $\gamma_T < 0.42$ and $q < 2.3 \times 10^{-4}$. Outside this gray region, the reduction target is faster (less than 10 hours) for large values of q ($q > 1.5 \times 10^{-4}$) and later (more than 75 hours) with low values of q ($q < 0.5 \times 10^{-4}$). The control parameter pair (p, q), in Figure 9(D), delimits a line below which control is not achieved. However above this limit line the reduction is reached more quickly as q increases. Indeed in this region, the color palette of the minimum period time control, varies from yellow to blue. For low values of q and p_T, in Figure 9(E), the pair of control parameters (q, p_T) does not achieve the 50% cancer cell reduction. However, increasing the q values makes it possible to achieve this reduction over a minimum period time going from more than 90 hours (red color) to less than 10 hours (blue color). In the case where (r_T, q) becomes the control parameter pair, as in Figure 9(F), the remission becomes really effective only if $q > 2 \times 10^{-4}$. In addition, the simultaneous increase in the values of r_T and q makes it possible to decrease the minimum time period for cancer reduction by 50%.
Our simulations also show that for a fixed choice of control parameter, estimating the minimum time peroid for cancer reduction greatly enhances in a synergistic fashion, the effectiveness of the control strategy..

4. Discussion and Conclusion

We have formulated in this work a mathematical model describing the interactions between the oncolytic virus, the tumor cells, the an-

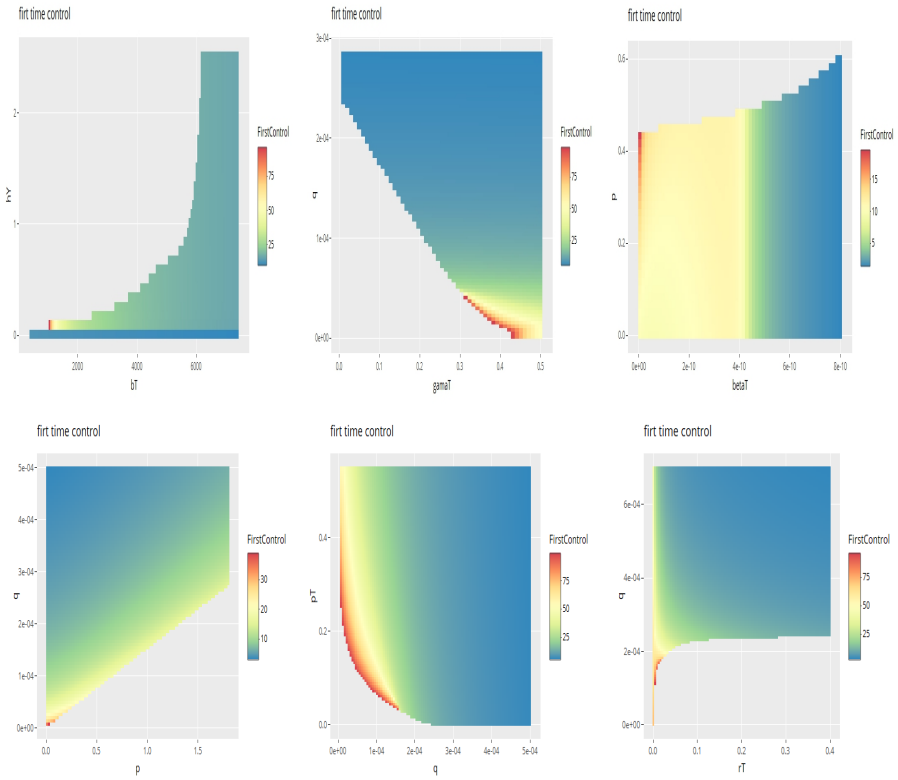

Figure 9: parameter space where the cancer reduction target is reached. The color palettes correspond to the minimum time to reach this control

titumoral and antiviral immune responses, by including inflammatory actions that contribute to both the stimulatory and inhibitory signals controlling the environmental capacity. The global sensitivity analysis in an inflammatory environment, showed strong variances, thus suggesting strong interactions between the parameters of the models. This sensitivity analysis also showed that the angiogenic inhibition stimulation parameters, integrated into the carrying capacity of cancer load, play an important role in the effectiveness of therapy. In particular, the carrying capacity inhibition coefficient most strongly influences the tumor proliferation.
Recent studies in vivo, suggest a positive benefit of combining an oncolytic virus with an anti-angiogenic agent in cancer treatment. In fact, Kurozumi et al. [26] found hat pretreatment of gliomas with the angiogenesis inhibitor cRGD peptide [56], reduced inflammation, vascular hyperpermeability, and leukocyte infiltration of tumor tissue upon treatment with the oncolytic virus hrR3. Reduction of host immune responses by cRGD treatment also enhanced the anticancer efficacy of oncolytic virus treatment by increasing oncolytic virus propagation in tumors. Kottke et al. [25] have demonstrated that combining VEGF165 inhibitors [32] with systemic delivery of oncolytic viruses leads to substantial regression and cure of established tumors in immunocompetent mice. This approach led to direct tumor cell lysis and triggered innate immunemediated attack on the tumor vasculature.

The sensitivity analysis has also revealed the key role played by the immune response in the tumor microenvironment (Figure 7). This matches the comments of de Graaf et al. [14] summarizing the benefits of onclyotic virus armed with immune modulators. In fact, they suggested in the case of inflamed tumors, hat responses of effector T cells and Natural Killer (NK) cells can be improved by immune activating agonists, such as 4-1BBL, and checkpoint inhibitors .

Given the growing importance of combination therapies, we evaluated whether there was synergism between anti-angiogenic treatment and gene therapy. Isobologram analysis showed, that over a 200-hour observation period, the existence of parameter regions leading to a reduction of 50% in tumor size was possible. In addition, we estimated the minimum time to reach this reduction target depending on the control parameters. Our simulations suggest that simultaneous variations of parameter pairs, having same or opposite effects on the dynamics of cancer cells display similar behavior to individual parameters in affecting nonlinear model output. We submit at this juncture that our results

provide a new way to achieve highly synergistic combinational strategy of anti-angiogenic treatment and gene therapy for cancer cell control. Furthermore, our analysis provides an estimate for the minimum period of time for cancer reduction in case of synergistic effects.

It is imperative from the sensitivity analysis of our model that employs the approach of combined anti-angiogenic and gene therapies provides new insights for effective overall cancer therapy. It opens up the possibility of an analytical approach to achieving remission or total extinction of cancer cells. It provides a tool for understanding how the combined effects of anti- angiogenic and gene therapies may be influenced by parameter variations and behaviors in inflammatory environments.

Finally, it yields insight into the robustness and stability of the target solutions for cancer reduction. At this point, we must remark that the rankings achieved especially by the inhibitory parameter q in the various scenarios leads us to conclude that the role played by inflammation, particularly in an anti-tumorigenic sense, suggests that this phenomenon cannot be ignored in cancer development and treatment.

Appendix

The method of Morris [31] derives measures of global sensitivity from a set of local derivatives, or elementary effects, sampled on a grid throughout the parameter space. The method of Morris is an extension of the traditional one-at-a-time (OAT) methods, in which each parameter x_i is perturbed along a grid of size Δ_i to create a trajectory through the parameter space. For a given model with d parameters, one trajectory will contain a sequence of p such perturbations. Each trajectory yields one estimate of the elementary effect for each parameter. Equation (3) shows the calculation of a single elementary effect for the i-th parameter :

$$EE_i = \frac{f(x_1, x_2, \cdots, x_i + \Delta_i, \cdots, x_d) - y}{\Delta_i}, \tag{3}$$

where $f(x)$ represents the prior point in the trajectory.

These elementary effects (EE) are evaluated at different points in the chosen input so that a large "dispersion" of the parameter space is explored and taken into account in the analysis. The obtained sample of all EE provide a measure of approximate overall importance, the mean and variance of the elementary effects. A high value of the mean

implies that a parameter is important, a high variance implies that its effects are non-linear or result from interactions with other inputs. This method does not separately evaluate the contribution of the interaction and the contribution of the parameters individually and gives the effects for each parameter which takes into account all the interactions and its individual contribution.

Morris global sensitivity analysis

In this section, the Morris method is investigated with different numbers of trajectories to identify the number of trajectories needed for a robust ranking of the parameters.
Results obtained from the Morris method yielded similar results compared to the Sobol's total effects sensitivity index, with regard to the parameter ranking and differentiation of important and non-influential parameters. The graphical representations in Figure 10 to Figure 15, illustrate our various results of parameter sensitivity analysis. According to the order of magnitude of the axis μ^*, we can establish a classification of the influence parameters. Interpretations concerning the non-linearity or the interaction level of the influence of all the parameters can be made in an analogous way by focusing on the plot of σ.

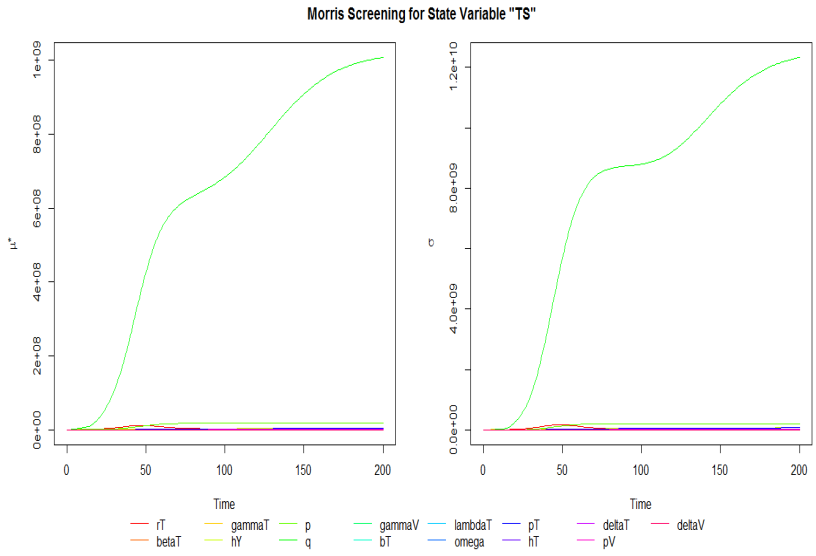

Figure 10: Morris screening for T_S state variable

In Figure 10, the Morris index indicates that the capacity inhibation coefficient q most strongly influence the population of susceptible and uninfected tumor cells, $T_S(t)$. Indeed, it has the greatest value μ^* throughout the study period. This same parameter is a factor involving non-linear interactions with the rest of the parameters. This same trend

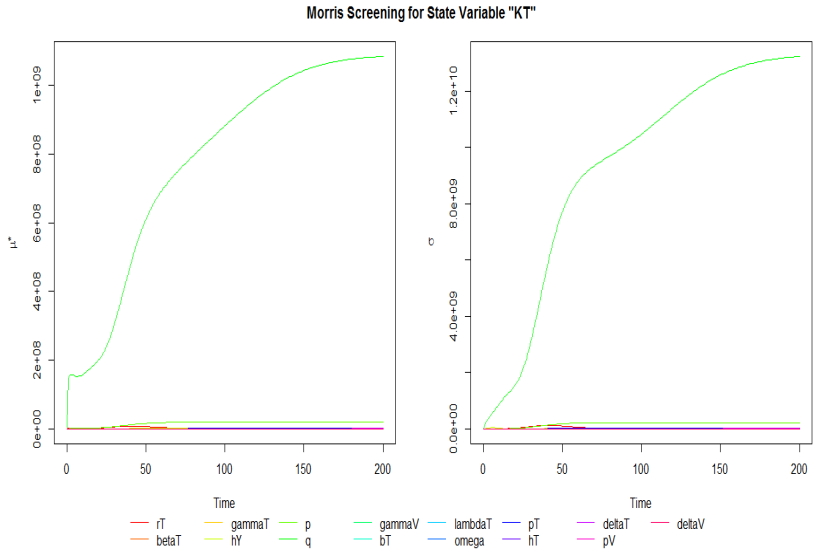

Figure 11: Morris screening for K_T state variable

for the parameter q is observed for the dynamics K_T during the 200 hours. The inhibition coefficient q is both the single of most influential parameter and factor of variability for non-linear interactions on the load capacity K_T (Figure 11). Figure 12 shows q, β_T and γ_V to be the most influential parameters on the population of infected tumor cells $T_I(t)$, but their relative importance changes during the simulation. In fact, q overtakes β_T and γ_V after a cap of 25 hours. The parameter γ_V will tend to lose its global influence on $T_I(t)$ in favor of the parameter ω from around 70 hours. It declines after 150 hours and close to 0 at the end of simulation.

It is important to highlight other parameters which have a significant global influences on $T_I(t)$ during the first 50 hours such as r_T, p_V, h_Y, p et λ_T. In addition, they also represent the overall parameters involving the most interactions and non-linearities on the dynamics of $T_I(t)$. In Figure 13, the virus clearance rate ω, represent the most influential parameter on the free-virus population size $V(t)$ and the key parameter concerning the non-linearity or the interaction level of influ-

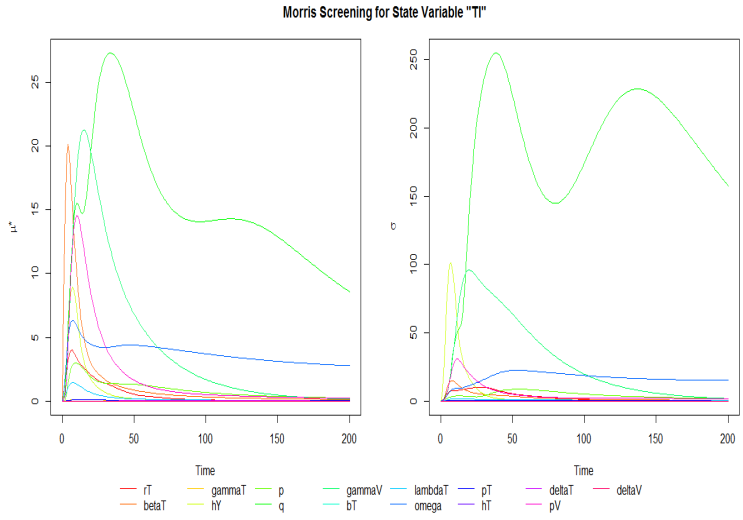

Figure 12: Morris screening for T_I state variable

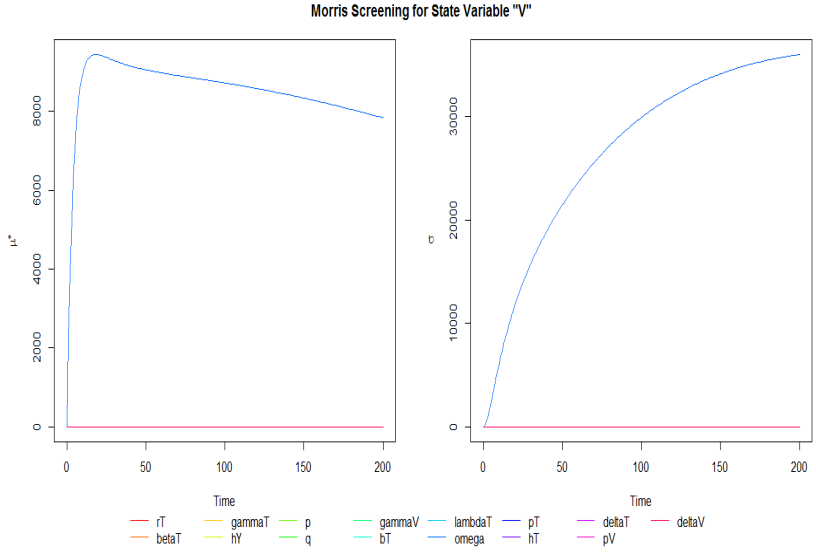

Figure 13: Morris screening for V state variable

ence among all other parameters. As seen in Figure 14, p_T and δ_T are far from the parameters that most affect the tumor-specific immune cells $Y_T(t)$. The p_T parameter gives way to the δ_T parameter from 140 hours. In addition, there are other non-negligible influence parameters, respectively h_Y, and few p on tumor-specific immune cells $Y_T(t)$. After

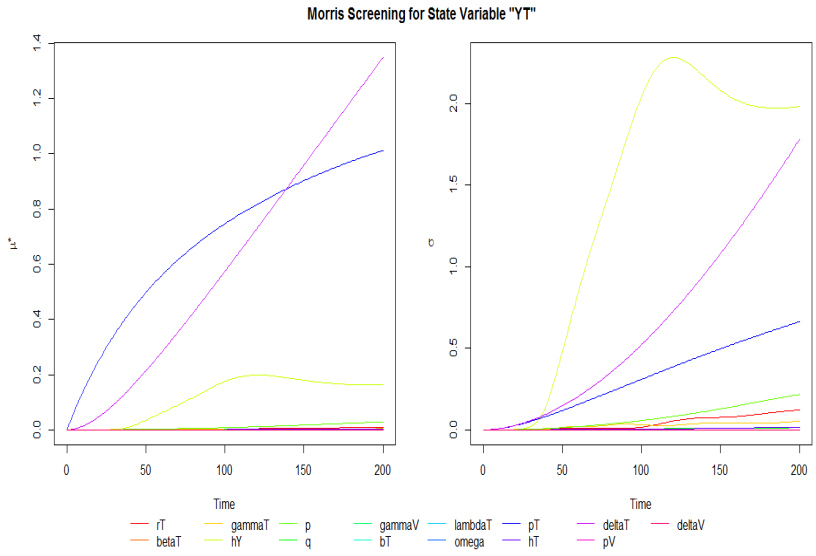

Figure 14: Morris screening for Y_T state variable

a cap of 30 hours, h_Y, δ_T and p_T are respectively the parameters that most induce non-linearity or level interaction of their influences on Y_T. Other parameters such as p, r_T and γ_T induce non- linearity or level interaction of their influences on Y_T. Also The graph for μ^* in Fig-

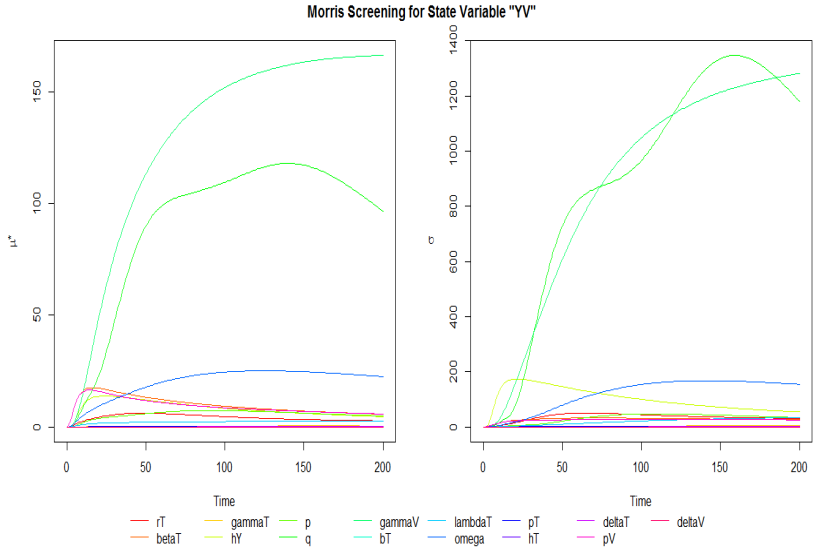

Figure 15: Morris screening for Y_V state variable

ure 15, reveals that the death rate from infected tumor cells, γ_V and the inhibation coefficient q have the greatest overall influence on the immune cells specific to the virus $Y_V(t)$. Interestingly, we notice that γ_V is closely followed by the parameter q. Other parameters of global influence on $Y_V(t)$ are respectively ω, p_V, β_T, q, p and r_T. Likewise, they are the ones that most imply non-linearity or the levels of influence interactions on $Y_V(t)$.

Analytical results

The non-trivial steady states of the model without virus (i.e., $T_I = Y_V = V = 0$) are described by

$$E_0 = (0, 0, 0, 0, 0, 0) \quad \text{Tumor-free steady state}$$

and

$$E_1 = (T_{S_0}, K_{T_0}, 0, 0, Y_{T_0}, 0) \quad \text{Tumor-only steady state}$$

with $K_{T_0} = \dfrac{p}{q} T_{S_0}^{1/3}$, $Y_{T_0} = \dfrac{p_T T_{S_0}}{\delta_T (h_T + T_{S_0})}$, and T_{S_0} is a solution of the following equation

$$aX^{5/3} + bX + cX^{2/3} - e = 0,$$

where

$$\begin{aligned} a &:= \frac{q}{p} r_T (\delta_T h_Y + p_T), \\ b &:= \gamma_T p_T - r_T (\delta_T h_Y + p_T), \\ c &:= \frac{q}{p} r_T \delta_T h_Y h_T, \\ e &:= r_T \delta_T h_Y h_T. \end{aligned}$$

In the presence of the virus, we deduce from the eqaution (1a) that $T_S = 0$ or

$$r_T \Big(1 - \frac{T_S + T_I}{K_T}\Big) - \beta_T V - \gamma_T \frac{Y_T}{h_Y + Y_T} = 0 \tag{4}$$

If $T_S = 0$, we have from eqaution (1b), that $T_I = 0$ or $T_I = (\dfrac{q}{p} K_T)^{-1/3}$. If $T_I = 0$, we have the following equilibrium point $E_2 = (0, K_T, 0, 0, 0, 0)$

and in this case, K_T is necessarily zero. So, $E_2 = E_0$.
If $T_I = (\frac{q}{p}K_T)^{-1/3}$, we have the following equilibrium point:

$$E_3 = \Big(0, K_T, (\frac{q}{p}K_T)^{-1/3}, \frac{b_T\lambda_T}{w}(\frac{q}{p}K_T)^{-1/3}, \frac{(\frac{q}{p}K_T)^{-1/3}}{h_T + (\frac{q}{p}K_T)^{-1/3}}, \frac{p_T}{\delta_V}(\frac{q}{p}K_T)^{-1/3}\Big).$$

In the case where $T_S \neq 0$, T_S ans T_I satisfy the following equation:

$$r_T - \frac{r_T q}{p}(T_S+T_I)^{2/3} - \beta_T\frac{b_T\lambda_T}{w}T_I - \frac{\gamma_T p_T(T_S+T_I)}{h_Y\delta_T(h_T+T_S+T_I)+p_T(T_S+T_I)} = 0$$

The Jacobian matrix J of the system (1a)–(1f) at any equilibria is written in this form:

$$\begin{bmatrix}
-\beta_T V - r_T(\frac{T_I+T_S}{K_T}-1) - \frac{Y_T\gamma_V}{Y_T+h_Y} - \frac{T_S r_T}{K_T} & \frac{r_T(T_I+T_S)T_S}{K_T^2} & -\frac{T_S r_T}{K_T} & -T_S\beta_T & -\frac{T_S\gamma_V}{Y_T+h_Y} + \frac{T_S Y_T\gamma_V}{(Y_T+h_Y)^2} & 0 \\
-\frac{2qK_T}{3(T_I+T_S)^{\frac{1}{3}}} + p & -q(T_I+T_S)^{\frac{2}{3}} & -\frac{2qK_T}{3(T_I+T_S)^{\frac{1}{3}}} + p & 0 & 0 & 0 \\
\beta_T V & 0 & -Y_V\gamma_V - \frac{Y_T\gamma_V}{Y_T+h_Y} - \lambda_S & T_S\beta_T & -\frac{T_I\gamma_V}{Y_T+h_Y} + \frac{T_I Y_T\gamma_V}{(Y_T+h_Y)^2} & -T_I\gamma_V \\
0 & 0 & b_T\lambda_T & -\omega & 0 & 0 \\
\frac{p_T}{T_I+T_S+h_T} - \frac{(T_I+T_S)p_T}{(T_I+T_S+h_T)^2} & 0 & \frac{p_T}{T_I+T_S+h_T} - \frac{(T_I+T_S)p_T}{(T_I+T_S+h_T)^2} & 0 & -\delta_T & 0 \\
0 & 0 & p_V(t-\tau) & 0 & 0 & -\delta_V
\end{bmatrix}$$

Acknowledgements

Our thanks to the anonymous referees whose valuable comments and suggestions aided in the revision of this paper.

[1] Abdalla, A., Xiao, L., Ullah, M. W., Yu, M., Ouyang, C., Yang, G. (2018). Current Challenges of Cancer Anti-angiogenic Therapy and the Promise of Nanotherapeutics, *Theranostics* 8 (2), 533–548. https://doi.org/10.7150/thno.21674

[2] Aghi, M., Rabkin, S. D., Martuza, R. L. (2007). Angiogenic response caused by oncolytic herpes simplex virus-induced reduced thrombospondin expression can be prevented by specific viral mutations or by administering a thrombospondin-derived peptide, *Cancer Res.*, 67 (2), 440–444. https://doi.org/10.1158/0008-5472.CAN-06-3145

[3] Aguilar-Cazares, D., Chavez-Dominguez, R., Carlos-Reyes, A., Lopez-Camarillo, C., Hernadez de la Cruz, O. N., Lopez-Gonzalez, J. S. (2019). Contribution of Angiogenesis to Inflammation and Cancer. *Frontiers in oncology, 9*, 1399. https://doi.org/10.3389/fonc.2019.01399

[4] Albini, A., Bruno, A., Noonan, D. M., Mortara, L. (2018). Contribution to Tumor Angiogenesis From Innate Immune Cells Within the Tumor Microenvironment: Implications for Immunotherapy. *Frontiers in immunology, 9*, 527. https://doi.org/10.3389/fimmu.2018.00527

[5] Ardaeva, A., Gatenby, R. A., Anderson, A., Byrne, H. M., Maini, P. K., Lorenzi, T. (2020). Evolutionary dynamics of competing phenotype-structured populations in periodically fluctuating environments. *Journal of mathematical biology, 80* (3), 775–807. https://doi.org/10.1007/s00285-019-01441-5

[6] Bernhauerov, V., Rezelj, V. V., Vignuzzi, M. (2020). Modelling Degradation and Replication Kinetics of the Zika Virus In Vitro Infection. *Viruses, 12* (5), 547. https://doi.org/10.3390/v12050547

[7] Blaylock, R. L. (2015). Cancer microenvironment, inflammation and cancer stem cells: A hypothesis for a paradigm change and new targets in cancer control. *Surgical neurology international, 6*, 92. https://doi.org/10.4103/2152-7806.157890

[8] Bouquet, C., Lamand, N., Brand, M., Gasc, J. M., Jullienne, B., Faure, G., Griscelli, F., Opolon, P., Connault, E., Perricaudet, M., Corvol, P. (2006). Suppression of angiogenesis, tumor growth, and metastasis by adenovirus-mediated gene transfer of human angiotensinogen. *Molecular therapy : the journal of the American Society of Gene Therapy, 14* (2), 175–182. https://doi.org/10.1016/j.ymthe.2006.01.017

[9] Bridle, B. W., Boudreau, J. E., Lichty, B. D., Brunellire, J., Stephenson, K., Koshy, S., Bramson, J. L., Wan, Y. (2009). Vesicular stomatitis virus as a novel cancer vaccine vector to prime antitumor immunity amenable to rapid boosting with adenovirus. *Molecular therapy : the journal of the American Society of Gene Therapy, 17* (10), 1814–1821. https://doi.org/10.1038/mt.2009.154

[10] Butturini, E., Carcereri de Prati, A., Boriero, D., Mariotto, S. (2019). Tumor Dormancy and Interplay with Hypoxic Tumor Microenvironment. *International journal of molecular sciences, 20* (17), 4305. https://doi.org/10.3390/ijms20174305

[11] Camara, B.I., Mokrani, H. (2012). Analysis of wave solutions of an adhenovirus-tumor cell system, *Abstract and Applied Analysis*, ID 590326 , 1–13. https://doi.org/10.1155/2012/590326

[12] Chen, D. G. (2009). A quantal statistical isobologram model to identify joint action for chemical mixtures, *Environmetrics*, 20: 101–109. https://doi.org/10.1002/env.918

[13] Csatary, L. K., Gosztonyi, G., Szeberenyi, J., Fabian, Z., Liszka, V., Bodey, B., Csatary, C. M. (2004). MTH-68/H oncolytic viral treatment in human high-grade gliomas. *Journal of neuro-oncology, 67* (1-2), 83–93. https://doi.org/10.1023/b:neon.0000021735.85511.05

[14] de Graaf, J. F., de Vor, L., Fouchier, R., van den Hoogen, B. G. (2018). Armed oncolytic viruses: A kick-start for anti-tumor immunity. *Cytokine & growth factor reviews, 41*, 28–39. https://doi.org/10.1016/j.cytogfr.2018.03.006

[15] de Pillis, L. G., Caldwell, T., Sarapata, E., Williams, H. (2013). Mathematical modeling of the regulatory T cell effects on renal cell carcinoma treatment, *Discrete and Continuous Dynamical Systems Series, 18* (4), 915–943. https://doi.org/10.3934/dcdsb.2013.18.915

[16] Eftimie, R., Dushoff, J., Bridle, B. W., Bramson, J. L., Earn, D. J. (2011). Multi-stability and multi-instability phenomena in a mathematical model of tumor-immune-virus interactions. *Bulletin of mathematical biology, 73* (12), 2932–2961. https://doi.org/10.1007/s11538-011-9653-5

[17] Friedman, A., Tao, Y. (2003). Analysis of a model of a virus that replicates selectively in tumor cells. *Journal of mathematical biology, 47* (5), 391–423. https://doi.org/10.1007/s00285-003-0199-5

[18] Friedman, A., Tian, J. P., Fulci, G., Chiocca, E. A., Wang, J. (2006). Glioma virotherapy: effects of innate immune suppression and increased viral replication capacity. *Cancer research, 66* (4), 2314–2319. https://doi.org/10.1158/0008-5472.CAN-05-2661

[19] Gujar, S., Pol, J. G., Kim, Y., Lee, P. W., Kroemer, G. (2018). Antitumor Benefits of Antiviral Immunity: An Underappreciated Aspect of Oncolytic Virotherapies. *Trends in immunology, 39* (3), 209–221. https://doi.org/10.1016/j.it.2017.11.006

[20] Haibe, Y., Kreidieh, M., El Hajj, H., Khalifeh, I., Mukherji, D., Temraz, S., Shamseddine, A. (2020). Resistance Mechanisms to Anti-angiogenic Therapies in Cancer. *Frontiers in oncology, 10*, 221. https://doi.org/10.3389/fonc.2020.00221

[21] Hanahan, D., Weinberg, R. A. (2011). Hallmarks of cancer: the next generation. *Cell, 144* (5), 646–674. https://doi.org/10.1016/j.cell.2011.02.013

[22] Hahnfeldt, P., Panigrahy, D., Folkman, J., Hlatky, L. (1999). Tumor development under angiogenic signaling: a dynamical theory of tumor growth, treatment response, and postvascular dormancy. *Cancer research, 59* (19), 4770–4775.

[23] Kimura, H., Braun, R. D., Ong, E. T., Hsu, R., Secomb, T. W., Papahadjopoulos, D., Hong, K., Dewhirst, M. W. (1996). Fluctuations in red cell flux in tumor microvessels can lead to transient hypoxia and reoxygenation in tumor parenchyma. *Cancer research, 56* (23), 5522–5528.

[24] Kirschner, D., Panetta, J. C. (1998). Modeling immunotherapy of the tumor-immune interaction. *Journal of mathematical biology, 37* (3), 235–252. https://doi.org/10.1007/s002850050127

[25] Kottke, T., Hall, G., Pulido, J., Diaz, R. M., Thompson, J., Chong, H., Selby, P., Coffey, M., Pandha, H., Chester, J., Melcher, A., Harrington, K., Vile, R. (2010). Antiangiogenic cancer therapy combined with oncolytic virotherapy leads to regression of established tumors in mice. *The Journal of clinical investigation, 120* (5), 1551–1560. https://doi.org/10.1172/JCI41431

[26] Kurozumi, K., Hardcastle, J., Thakur, R., Yang, M., Christoforidis, G., Fulci, G., Hochberg, F. H., Weissleder, R., Carson, W., Chiocca, E. A., Kaur, B. (2007). Effect of tumor microenvironment modulation on the efficacy of oncolytic virus therapy. *Journal of the National Cancer Institute, 99* (23), 1768–1781. https://doi.org/10.1093/jnci/djm229

[27] Mahasa, K. J., Eladdadi, A., de Pillis, L., Ouifki, R. (2017). Oncolytic potency and reduced virus tumor-specificity in oncolytic virotherapy. A mathematical modelling approach. *PloS one, 12* (9), e0184347. https://doi.org/10.1371/journal.pone.0184347

[28] Mak, S. (1971). Defective virions in human adenovirus type 12. *Journal of virology, 7* (4), 426–433. https://doi.org/10.1128/JVI.7.4.426-433.1971

[29] Marelli, G., Howells, A., Lemoine, N. R., Wang, Y. (2018). Oncolytic Viral Therapy and the Immune System: A Double-Edged Sword Against Cancer. *Frontiers in immunology, 9*, 866. https://doi.org/ 10.3389/fimmu.2018.00866

[30] Moore, J. L., Liang, S., Akullian, A., Remais, J. V. (2012). Cautioning the use of degree-day models for climate change projections in the presence of parametric uncertainty. *Ecological applications : a publication of the Ecological Society of America, 22* (8), 2237–2247. https://doi.org/10.1890/12-0127.1

[31] Morris, M. D. (1991). Factorial sampling plans for preliminary computational experiments, *Technometrics, 33* (2), 161–174. https://doi.org/10.2307/1269043

[32] Niu, G., Chen, X. (2010). Vascular endothelial growth factor as an anti-angiogenic target for cancer therapy. *Current drug targets, 11* (8), 1000–1017. https://doi.org/10.2174/138945010791591395

[33] Nossent, J., Elsen, P., Bauwens, W. (2011). Sobol' sensitivity analysis of a complex environmental model. *Environmental Modelling & Software, 26* (12), 1515–1525. https://doi.org/10.1016/j.envsoft.2011.08.010

[34] Okas, C., Roche, S., Krzinger, M. L., Riche, B., Bricout, H., Derrough, T., Simondon, F., Ecochard, R. (2010). Methodology of the sensitivity analysis used for modeling an infectious disease. *Vaccine, 28* (51), 8132–8140. https://doi.org/10.1016/j.vaccine.2010.09.099

[35] Okamoto, K. W., Amarasekare, P., Petty, I. T. (2014). Modeling oncolytic virotherapy: is complete tumor-tropism too much of a good thing?. *Journal of theoretical biology, 358*, 166–178. https://doi.org/10.1016/j.jtbi.2014.04.030

[36] Paiva, L. R., Binny, C., Ferreira, S. C., Jr, Martins, M. L. (2009). A multiscale mathematical model for oncolytic virotherapy. *Cancer research, 69* (3), 1205–1211. https://doi.org/10.1158/0008-5472.CAN-08-2173

[37] Prabha, S., Sharma, B., Labhasetwar, V. (2012). Inhibition of tumor angiogenesis and growth by nanoparticle-mediated p53 gene therapy in mice. *Cancer gene therapy, 19* (8), 530–537. https://doi.org/10.1038/cgt.2012.26

[38] Qian, G., Mahdi, A. (2020). Sensitivity analysis methods in the biomedical sciences. *Mathematical biosciences, 323*, 108306. https://doi.org/10.1016/j.mbs.2020.108306

[39] Saltelli, A., Annoni, P., Azzini, I., Campolongo, F., Ratto, M., Tarantola, S. (2010). Variance based sensitivity analysis of model output. Design and estimator for the total sensitivity index. *Computer Physics Communications, 181* (2), 259–270. https://doi.org/10.1016/j.cpc.2009.09.018.

[40] Sobol, I. M. (1990). On sensitivity estimates for nonlinear mathematical models, *Matematicheskoe Modelirovanie, 2* (1), 112–118.

[41] Storey, K. M., Lawler, S. E., Jackson, T. L. (2020). Modeling Oncolytic Viral Therapy, Immune Checkpoint Inhibition, and the Complex Dynamics of Innate and Adaptive Immunity in Glioblastoma Treatment. *Frontiers in physiology, 11*, 151. https://doi.org/10.3389/fphys.2020.00151

[42] Streby, K. A., Geller, J. I., Currier, M. A., Warren, P. S., Racadio, J. M., Towbin, A. J., Vaughan, M. R., Triplet, M., Ott-Napier, K., Dishman, D. J., Backus, L. R., Stockman, B., Brunner, M., Simpson, K., Spavin, R., Conner, J., Cripe, T. P. (2017). Intratumoral Injection of HSV1716, an Oncolytic Herpes Virus, Is Safe and Shows Evidence of Immune Response and Viral Replication in Young Cancer Patients. *Clinical cancer research : an official journal of the American Association for Cancer Research, 23* (14), 3566–3574. https://doi.org/10.1158/1078-0432.CCR-16-2900

[43] Takayanagi, T., Ohuchi, A. (2001). A Mathematical analysis of the interactions between immunogenic cells and cytotoxic T Lymphocytes, *Microbiology and immunology, 45*, (10), 709–715. https://doi.org/10.1111/j.1348-0421.2001.tb01305.x

[44] Toumi, H., Boumaiza, M., Millet, M., Radetski, C. M., Camara, B. I., Felten, V., Masfaraud, J. F., Frard, J. F. (2018). Combined acute ecotoxicity of malathion and deltamethrin to Daphnia magna (Crustacea, Cladocera): comparison of different data analysis approaches. *Environmental science and pollution research international, 25* (18), 1778117788. https://doi.org/10.1007/s11356-018-1909-2

[45] Voronov, E., Shouval, D. S., Krelin, Y., Cagnano, E., Benharroch, D., Iwakura, Y., Dinarello, C. A., Apte, R. N. (2003). IL-1 is required

for tumor invasiveness and angiogenesis. *Proceedings of the National Academy of Sciences of the United States of America, 100* (5), 2645–2650. https://doi.org/10.1073/pnas.0437939100

[46] Wang, Y., Qiu, H., Hu, W., Li, S., Yu, J. (2014). Over-expression of platelet-derived growth factor-D promotes tumor growth and invasion in endometrial cancer. *International journal of molecular sciences, 15* (3), 4780–4794. https://doi.org/10.3390/ijms15034780

[47] Wang, L., Schmitz, V., Perez-Mediavilla, A., Izal, I., Prieto, J., Qian, C. (2003). Suppression of angiogenesis and tumor growth by adenoviral-mediated gene transfer of pigment epithelium-derived factor. *Molecular therapy : the journal of the American Society of Gene Therapy, 8* (1), 72–79. https://doi.org/10.1016/s1525-0016(03)00128-x

[48] Wilkie, K. P., Hahnfeldt, P. (2017). Modeling the Dichotomy of the Immune Response to Cancer: Cytotoxic Effects and Tumor-Promoting Inflammation. *Bulletin of mathematical biology, 79* (6), 1426–1448. https://doi.org/10.1007/s11538-017-0291-4

[49] Wilkie, K. P., Aktar, F. (2020). Mathematically modelling inflammation as a promoter of tumour growth. *Mathematical medicine and biology : a journal of the IMA, 37* (4), 491–514. https://doi.org/10.1093/imammb/dqaa005

[50] Wong, H. H., Lemoine, N. R., Wang, Y. (2010). Oncolytic Viruses for Cancer Therapy: Overcoming the Obstacles. *Viruses, 2* (1), 78–106. https://doi.org/10.3390/v2010078

[51] Wodarz, D., Komarova, N. (2005). Computational Biology Of Cancer: Lecture Notes And Mathematical Modeling, in *World Scientific Publishing Company*, Singapore. https://doi.org/10.1142/5642

[52] Wodarz, D. (2001). Viruses as antitumor weapons: defining conditions for tumor remission. *Cancer research, 61* (8), 3501–3507.

[53] Wu, J., Dhingra, R., Gambhir, M., Remais, J. V. (2013). Sensitivity analysis of infectious disease models: methods, advances and their application. *Journal of the Royal Society, Interface, 10* (86), 20121018. https://doi.org/10.1098/rsif.2012.1018

[54] Wu, J. T., Kirn, D. H., Wein, L. M. (2004). Analysis of a three-way race between tumor growth, a replication-competent virus and

an immune response. *Bulletin of mathematical biology, 66* (4), 605–625. https://doi.org/10.1016/j.bulm.2003.08.016

[55] Wu, J. T., Byrne, H. M., Kirn, D. H., Wein, L. M. (2001). Modeling and analysis of a virus that replicates selectively in tumor cells. *Bulletin of mathematical biology, 63* (4), 731–768. https://doi.org/10.1006/bulm.2001.0245

[56] Yamada, S., Bu, X. Y., Khankaldyyan, V., Gonzales-Gomez, I., McComb, J. G., Laug, W. E. (2006). Effect of the angiogenesis inhibitor Cilengitide (EMD 121974) on glioblastoma growth in nude mice. *Neurosurgery, 59* (6), 1304–1312. https://doi.org/10.1227/01.NEU.0000245622.70344.BE

[57] Yang, L. P., Cheng, P., Peng, X. C., Shi, H. S., He, W. H., Cui, F. Y., Luo, S. T., Wei, Y. Q., Yang, L. (2009). Anti-tumor effect of adenovirus-mediated gene transfer of pigment epithelium-derived factor on mouse B16-F10 melanoma. *Journal of experimental & clinical cancer research : CR, 28* (1), 75. https://doi.org/10.1186/1756-9966-28-75